

The polarization and the fundamental sensitivity of ^{39}K (^{133}Cs)- ^{85}Rb - ^4He hybrid optical pumping spin exchange relaxation free atomic magnetometers

Jian-Hua Liu^{1,2}, Dong-Yang Jing¹, Liang-Liang Wang¹, Pei-Song He², Wei Quan³, Jian-Cheng Fang³, Wu-Ming Liu^{†,1}

The hybrid optical pumping spin exchange relaxation free (SERF) atomic magnetometers can realize ultrahigh sensitivity measurement of magnetic field and inertia. We have studied the ^{85}Rb polarization of two types of hybrid optical pumping SERF magnetometers based on ^{39}K - ^{85}Rb - ^4He and ^{133}Cs - ^{85}Rb - ^4He (^{39}K (^{133}Cs)- ^{85}Rb - ^4He magnetometers), then found that the polarization of ^{85}Rb varies with the number density of buffer gas (^4He) and quench gas (N_2), the optical pumping rate of pump beam and cell temperature respectively, which will provide an experimental guide for the design of the hybrid optical pumping SERF magnetometer. We obtain a general formula on the fundamental sensitivity of the hybrid optical pumping SERF magnetometer due to the shot-noise of a probe laser, which describes that the fundamental sensitivity of the magnetometer varies with the number density of buffer gas and quench gas, the optical pumping rate of pump beam, external magnetic field, cell effective radius, measurement volume, cell temperature and measurement time. We obtain a highest fundamental sensitivity of $26.303aT/\text{Hz}^{1/2}$ ($1aT = 10^{-18}\text{T}$) with ^{39}K - ^{85}Rb - ^4He magnetometer among above two types of magnetometers when the polarization of ^{85}Rb atom is 0.0121. Optimizing the magnetometer parameters is advantageous to improve the sensitivity of the hybrid optical pumping SERF magnetometer in measuring weak magnetic field.

We estimate the fundamental sensitivity limit of the hybrid optical pumping SERF magnetometer to be superior to $1.8449 \times 10^{-2} aT/Hz^{1/2}$, which is higher than the shot-noise-limited sensitivity of $1aT/Hz^{1/2}$ of K SERF atomic magnetometer.

¹*Beijing National Laboratory for Condensed Matter Physics, Institute of Physics, Chinese Academy of Sciences, Beijing 100190, China*

²*School of Science, Beijing Technology and Business University, Beijing 100048, China*

³*School of Instrument Science and Opto-electronics Engineering, Beihang University, Beijing 100191, China*

[†]e-mail: wliu@iphy.ac.cn

In recent years, ultrahigh sensitive magnetic field measurement technology has become a hotspot in research of weak magnetic field. In the field of biomedicine, it is used in magnetoencephalography (MEG) and magnetocardiography (MCG)¹⁻³. In physics, it is used to analyze the magnetism of material and measure the symmetry broken of charge conjugation, parity transformation and time reversal (CPT)⁴⁻⁶. At present, the sensitivity of the spin exchange relaxation free (SERF) atomic magnetometer is the highest in the ultrahigh sensitive magnetometers^{3,7-10}. The effects of the spin-exchange relaxation can be suppressed in the SERF regime, when the spin-exchange rate is much larger than the Larmor precession frequency^{11,12}. The SERF regime can be reached by operating with sufficiently high alkali metal number density (at higher temperature) and in sufficiently low magnetic field^{12,13}.

It was found that hybrid optical pumping can make the SERF magnetometer realize higher experimental detecting sensitivity and more homogeneous atomic spin polarization¹⁴ and it is suitable for quantum nondestructive measurement¹⁵. Ito et al.^{16,17} realized a sensitivity of $3 \times 10^4 aT/Hz^{1/2}$ in magnetic field measurement by SERF atomic magnetometers by hybrid optical pumping of K-Rb. Fang et al.¹⁸ obtained a sensitivity of approximately $5 \times 10^3 aT/Hz^{1/2}$ by optimizing the parameters of SERF magnetometer based on K-Rb hybrid optical pumping. Li et al.¹⁹ measured the magnetic field sensitivity better than $700 aT/Hz^{1/2}$ by a subfemtotesla atomic magnetometer based on hybrid optical pumping of K-Rb. However, there is almost no work about the systematic analysis of the influence factors on the polarization and the fundamental sensitivity of K (Cs)-Rb-He (Ne) hybrid optical pumping SERF atomic magnetometers. We need more practical methods to obtain higher fundamental sensitivity of the hybrid optical pumping SERF atomic magnetometer.

In this report, we obtain a general formula on the fundamental sensitivity of the hybrid optical pumping SERF magnetometer, which describes the fundamental sensitivity of the magnetometer vary with the number density of buffer gas and quench gas, optical pumping rate of pump beam, external magnetic field, cell effective radius, measurement volume, cell temperature and measurement time. We have investigated two types of hybrid optical pumping SERF atomic magnetometers based on ^{39}K (^{133}Cs)- ^{85}Rb - ^4He (^{39}K (^{133}Cs)- ^{85}Rb - ^4He magnetometers), then found the fundamental sensitivity of ^{133}Cs - ^{85}Rb - ^4He magnetometer is lower than the one of ^{39}K - ^{85}Rb - ^4He magnetometer at the same cell temperature. Furthermore, we obtained a higher fundamental sensitivity of $1.8449 \times 10^{-2} aT/Hz^{1/2}$ with ^{39}K - ^{85}Rb - ^4He magnetometer when the polarization of ^{85}Rb atom is 1.3961×10^{-5} and the fundamental sensitivity is higher than the shot-noise-limited sen-

sitivity of K SERF atomic magnetometer¹⁰ in the range $10 - 1aT/Hz^{1/2}$. Among ³⁹K, ⁸⁵Rb and ¹³³Cs, the number density of ³⁹K is affected least by temperature, so the SERF magnetometer based on ³⁹K is suitable for an environment with the temperature varying drastically. These findings not only optimize the parameters for the SERF regime, but also provide an experimental guide for the design of the hybrid optical pumping SERF magnetometer.

Results

The number density of alkali-metal atoms. The alkali metal gas cell of the SERF atomic magnetometer based on hybrid optical pumping contains two types of alkali metal atoms, they are ³⁹K-⁸⁵Rb or ¹³³Cs-⁸⁵Rb. ¹³³Cs can reach large saturation vapor pressure at lower temperature²⁰ and realize SERF regime at lower temperature, which has more advantages for low temperature conditions. ³⁹K has the highest theoretical sensitivity, so we study the hybrid optical pumping SERF atomic magnetometer based on of ³⁹K-⁸⁵Rb or ¹³³Cs-⁸⁵Rb. We select ⁴He as the buffer gas and take N₂ as quench gas (that is ³⁹K (¹³³Cs)-⁸⁵Rb-⁴He magnetometers). One type of alkali-metal atom which is directly pumped and polarized by a circularly polarized pump beam is called A and the other type of alkali-metal atom which is polarized by the spin-exchange collisions with A is called B in the hybrid optical pumping SERF magnetometer^{15,21}, we take ³⁹K and ¹³³Cs as A respectively, select ⁸⁵Rb as B in the SERF regime. The number density of alkali-metal vapor and the polarization of alkali-metal vapor are two of the most important parameters of the cell²².

The relation between the number density of alkali-metal atoms and cell temperature is given

by⁵

$$n = \frac{1}{T} 10^{21.866 + A_1 - B_1/T}, \quad (1)$$

where n is the number density of alkali-metal (³⁹K, ⁸⁵Rb and ¹³³Cs) atom in cm^{-3} , T is temperature in Kelvin, the parameters A_1 and B_1 are number density parameters²⁰, where $A_1^K = 4.402$, $A_1^{Rb} = 4.312$, $A_1^{Cs} = 4.165$, $B_1^K = 4453$, $B_1^{Rb} = 4040$ and $B_1^{Cs} = 3830$ for the temperature is higher than $400K$.

We can obtain the number density of ³⁹K, ¹³³Cs and ⁸⁵Rb vary with temperature from Eq. (1) as shown in Fig. 1. When the number density of ³⁹K, ⁸⁵Rb and ¹³³Cs atom are the same, ³⁹K need the highest temperature. Moreover, the effect of temperature on the number density of ³⁹K is the minimum, so ³⁹K is applicable to the working environment when temperature varies drastically. In general, the number density of the alkali metal atoms is $10^{13}cm^{-3}$ to $10^{14}cm^{-3}$ in the SERF regime. When $T = 457.5K$, $n_K = 7.4864 \times 10^{13}cm^{-3}$, $n_{Rb} = 9.9776 \times 10^{14}cm^{-3}$, $n_{Cs} = 4.8642 \times 10^{14}cm^{-3}$. $T = 457.6K$, $n_K = 7.5216 \times 10^{13}cm^{-3}$, $n_{Rb} = 1.0017 \times 10^{15}cm^{-3}$, $n_{Cs} = 4.8848 \times 10^{14}cm^{-3}$. We choose $T = 457.5K$ as the highest temperature in the SERF regime.

The polarization of alkali-metal atom. Considering the spin-exchange between two types of alkali-metal atoms, the spin polarization P of each type of atoms can be described as²³,

$$P_A = \frac{R_A}{R_A + \Gamma_A + k_{SE}n_B}, \quad (2)$$

$$P_B = \frac{k_{SE}n_A P_A}{\Gamma_B + k_{SE}n_A}, \quad (3)$$

$$\Gamma_A = n_A \sigma_{SD}^{A-A} \bar{v}_{A-A} + n_{He} \sigma_{SD}^{A-He} \bar{v}_{A-He} + n_{N_2} \sigma_{SD}^{A-N_2} \bar{v}_{A-N_2} + n_A \sigma_{SD}^{A-B} \bar{v}_{A-B}, \quad (4)$$

$$\Gamma_B = n_B \sigma_{SD}^{B-B} \bar{v}_{B-B} + n_{He} \sigma_{SD}^{B-He} \bar{v}_{B-He} + n_{N_2} \sigma_{SD}^{B-N_2} \bar{v}_{B-N_2} + n_B \sigma_{SD}^{B-A} \bar{v}_{B-A}, \quad (5)$$

where R_A is the pump beam optical pumping rate of atom A, which is mainly determined by pumping laser parameters⁶, $R_B = k_{SE} n_A P_A$ is the pumping rate of atom B, Γ is the spin destruction relaxation rate, k_{SE} is the spin-exchange rate constant, n is the number density of atoms, R_{SE}^{A-B} is the spin-exchange rate of atom A with atom B, $R_{SE}^{A-B} = k_{SE} n_B$, $\bar{v}_{alkali-alkali}$ is the thermal velocity of the alkali atoms, $\bar{v}_{alkali-alkali} = \sqrt{\frac{8\kappa_B T}{\pi m_{alkali-alkali}}}$, $\bar{v}_{alkali-N_2} = \sqrt{\frac{8\kappa_B T}{\pi m_{alkali-N_2}}}$ is the thermal velocity of the alkali atoms and quench gas N₂ respectively, the reduced mass of alkali atoms and quench gas N₂ is $m_{alkali-N_2} = \frac{m_{alkali}m_{N_2}}{m_{alkali}+m_{N_2}}$, the thermal velocity of the alkali atoms and buffer gas ⁴He is $\bar{v}_{alkali-He} = \sqrt{\frac{8\kappa_B T}{\pi m_{alkali-He}}}$, the reduced mass of alkali atoms and buffer gas ⁴He is $m_{alkali-He} = \frac{m_{alkali}m_{He}}{m_{alkali}+m_{He}}$, k_{SE} for different alkali metal atoms are nearly the same²⁴⁻²⁸, mean $k_{SE} = \langle \sigma_{SE} v \rangle$, $k_{SE}^{Rb-Cs} \approx k_{SE}^{Cs-Rb}$, $k_{SE}^{Rb-K} \approx k_{SE}^{K-Rb}$, we get $k_{SE}^{Cs-Rb} = \sigma_{SE}^{Cs-Rb} \sqrt{\frac{m_{Rb}+m_{Cs}}{m_{Rb}m_{Cs}}} \sqrt{\frac{8\kappa_B T}{\pi}}$ and $k_{SE}^{K-Rb} = \sigma_{SE}^{K-Rb} \sqrt{\frac{m_{Rb}+m_K}{m_{Rb}m_K}} \sqrt{\frac{8\kappa_B T}{\pi}}$, where $\sigma_{SE}^{K-Rb} \approx \sigma_{SE}^{Rb-Cs} \approx 2 \times 10^{-14} \text{ cm}^2$, σ_{SE}^{K-Rb} is the spin-exchange cross section of ³⁹K and ⁸⁵Rb by spin-exchange collisions with each other, σ_{SE}^{Cs-Rb} is the spin-exchange cross section of ¹³³Cs and ⁸⁵Rb by spin-exchange collisions with each other, σ_{SD}^{K-Rb} is the spin-destruction cross section of ³⁹K and ⁸⁵Rb by collisions with each other, $\sigma_{SD}^{K-Rb} = \sigma_{SD}^{Rb-K} = 1 \times 10^{-18} \text{ cm}^2$, σ_{SD}^{Cs-Rb} is the spin-destruction cross section of ¹³³Cs and ⁸⁵Rb by collisions with each other, $\sigma_{SD}^{Cs-Rb} = \sigma_{SD}^{Rb-Cs} = 1.6 \times 10^{-17} \text{ cm}^2$.

A represents ³⁹K or ¹³³Cs, B represents ⁸⁵Rb. κ_B is Boltzmann's constant, T is cell temperature, the spin-exchange cross section of ³⁹K, ⁸⁵Rb and ¹³³Cs is $\sigma_{SE}^K = 1.8 \times 10^{-14} \text{ cm}^2$, $\sigma_{SE}^{Rb} = 1.9 \times 10^{-14} \text{ cm}^2$ and $\sigma_{SE}^{Cs} = 2.1 \times 10^{-14} \text{ cm}^2$ respectively^{25,30}, the spin-destruction cross

section of ^{39}K , ^{85}Rb and ^{133}Cs is $\sigma_{SD}^K = 1 \times 10^{-18} \text{cm}^2$, $\sigma_{SD}^{Rb} = 1.6 \times 10^{-17} \text{cm}^2$ and $\sigma_{SD}^{Cs} = 2 \times 10^{-16} \text{cm}^2$ respectively^{29,31}, the spin-destruction cross section of ^4He and ^{39}K , ^4He and ^{85}Rb , ^4He and ^{133}Cs is $\sigma_{SD}^{K-He} = 8 \times 10^{-25} \text{cm}^2$, $\sigma_{SD}^{Rb-He} = 9 \times 10^{-24} \text{cm}^2$ and $\sigma_{SD}^{Cs-He} = 2.8 \times 10^{-23} \text{cm}^2$ respectively³². The spin-destruction cross section of N_2 and ^{39}K , N_2 and ^{85}Rb , N_2 and ^{133}Cs is $\sigma_{SD}^{K-N_2} = 7.9 \times 10^{-23} \text{cm}^2$, $\sigma_{SD}^{Rb-N_2} = 1 \times 10^{-22} \text{cm}^2$ and $\sigma_{SD}^{Cs-N_2} = 5.5 \times 10^{-22} \text{cm}^2$ respectively^{29,32}.

Substitute Eq. (2) into Eq. (3) and we consider the spin exchange between same atoms, we obtain

$$P_B = \frac{R_A k_{SE}^{A-B} n_A}{(\Gamma_B + k_{SE}^{B-A} n_A + k_{SE}^{B-B} n_B)(R_A + \Gamma_A + k_{SE}^{A-B} n_B + k_{SE}^{A-A} n_A)}, \quad (6)$$

We take one of n_{He} , n_{N_2} , T , R_A and cell temperature by Eq. (6) as a variable (other parameters are invariable) to obtain the results that the polarization of the hybrid optical pumping SERF magnetometer based on ^{39}K (^{133}Cs)- ^{85}Rb - ^4He respectively vary with the variable, where $n_{He} = 10^{19} \text{cm}^{-3}$, $n_{N_2} = 2 \times 10^{17} \text{cm}^{-3}$, $R_A = R_A^K = R_A^{Cs} = 200000 \text{s}^{-1}$, when $T = 457.5 \text{K}$, $n_K = 7.4864 \times 10^{13} \text{cm}^{-3}$, $n_{Rb} = 9.9776 \times 10^{14} \text{cm}^{-3}$, $n_{Cs} = 4.8642 \times 10^{14} \text{cm}^{-3}$, at the moment, ^{39}K , ^{85}Rb and ^{133}Cs are in the SERF regime.

The number density of ^{39}K , ^{85}Rb and ^{133}Cs vary with cell temperature, so the relation among the polarization of ^{85}Rb , the number density of ^{39}K , ^{85}Rb and ^{133}Cs , cell temperature is nonlinear in group ^{39}K - ^{85}Rb and ^{133}Cs - ^{85}Rb . At the same cell temperature, the number density of ^{39}K , ^{85}Rb and ^{133}Cs are different. When the number density of ^{39}K , ^{85}Rb and ^{133}Cs are equivalent, the cell temperature of ^{39}K - ^{85}Rb and ^{133}Cs - ^{85}Rb magnetometers are different, and the ^{85}Rb polarization of

^{39}K - ^{85}Rb and ^{133}Cs - ^{85}Rb magnetometers are also different.

Fig. 2 show the ^{85}Rb polarization of ^{39}K (^{133}Cs)- ^{85}Rb - ^4He magnetometers as a function of ^{39}K , ^{133}Cs , ^{85}Rb , ^4He , and N_2 number density, the optical pumping rate of pump beam and cell temperature, including the effects of spin exchange due to ^{39}K - ^{39}K , ^{39}K - ^{85}Rb , ^{85}Rb - ^{85}Rb , ^{133}Cs - ^{85}Rb , ^{133}Cs - ^{133}Cs and spin relaxation due to ^{39}K - ^{39}K , ^{39}K - ^{85}Rb , ^{85}Rb - ^{85}Rb , ^{133}Cs - ^{85}Rb , ^{133}Cs - ^{133}Cs , ^{39}K - ^4He , ^{85}Rb - ^4He , ^{133}Cs - ^4He collisions, ^{39}K - N_2 , ^{85}Rb - N_2 , ^{133}Cs - N_2 destructions. The ^{85}Rb polarization almost does not vary with the number density of ^4He when the number density of ^4He is smaller than a critical value 10^{22}cm^{-3} in ^{39}K - ^{85}Rb - ^4He (black line in squares) and 10^{21}cm^{-3} in ^{133}Cs - ^{85}Rb - ^4He (red line in dots), otherwise, the ^{85}Rb polarization decreases rapidly in (a). The ^{85}Rb polarization almost does not vary with the number density of N_2 when the number density of N_2 is smaller than $2 \times 10^{21}\text{cm}^{-3}$ for ^{39}K - ^{85}Rb - ^4He magnetometer and $2 \times 10^{20}\text{cm}^{-3}$ for ^{133}Cs - ^{85}Rb - ^4He magnetometer. Otherwise, the polarization of ^{85}Rb decreases rapidly in (b). (c) The ^{85}Rb polarization increases with the increasing optical pumping rate of pump beam R_A^K and R_A^{Cs} respectively. The polarization of ^{85}Rb decreases with the cell temperature increasing in (d). The polarization of ^{85}Rb of ^{133}Cs - ^{85}Rb - ^4He magnetometer is bigger than the one of ^{39}K - ^{85}Rb - ^4He magnetometer in (a)-(d).

The fundamental sensitivity of the hybrid optical pumping SERF atomic magnetometer. To improve the practicability of the hybrid optical pumping SERF atomic magnetometer, it is necessary to improve the sensitivity and stability of the magnetometer and realize the miniaturization of the magnetometer. The fundamental, shot-noise-limited sensitivity of the SERF atomic magne-

tometer is given by³³

$$\delta B = \frac{1}{\gamma_e \sqrt{n T_2 V t}}, \quad (7)$$

it is also the ultimate sensibility of the SERF atomic magnetometer³², where n is the number density of atoms, γ_e is electron gyromagnetic ratio, $\gamma_e = \frac{g\mu_B}{\hbar}$, V is the measurement volume, t is the measurement time, T_2 is the transverse spin relaxation time⁸, $\frac{1}{T_2} = \Gamma_A + \Gamma_B + R_{wall}^A + R_{wall}^B + R_{SE}^{ee}$, R_{wall} is the relaxation rate due to the alkali-metal atoms diffusion to the walls⁶, $R_{wall} = q(P) D_0 \left(\frac{\sqrt{1+T/273.15}}{P_{buffer}/1amg} \right) \left(\frac{\pi}{a} \right)^2$, $q(P)$ is the nuclear slowing-down factor of alkali-metal atom³⁴, $q(P)_K = \frac{6+2P^2}{1+P^2}$ for ³⁹K atom, $q(P)_{Rb} = \frac{38+52P^2+6P^4}{3+10P^2+3P^4}$ for ⁸⁵Rb atom, $q(P)_{Cs} = \frac{22+70P^2+34P^4+2P^6}{1+7P^2+7P^4+P^6}$ for ¹³³Cs atom, D_0 is the diffusion constant of the alkali atom within the buffer gas³⁵⁻³⁷ in units of cm^2/s and is given at 1amg and 273K, $1amg = 2.69 \times 10^{19} cm^{-3}$, $D_0 (K - He) = 0.35 cm^2/s$, $D_0 (Rb - He) = 0.5 cm^2/s$, $D_0 (Cs - He) = 0.29 cm^2/s$, P_{buffer} is the pressure intensity of buffer gas in amg, a is the equivalent radius of the gas cell, $a = 1cm$, R_{SE}^{ee} is the relaxation rate due to alkali-alkali spin-exchange collisions³⁸, here we have $R_{SE}^{ee} = R_{SE}^{AA} + R_{SE}^{AB} + R_{SE}^{BA} + R_{SE}^{BB}$, $R_{SE}^{AA} = \left(\frac{g\mu_B B}{q(0)_A \hbar} \right)^2 \frac{q(0)_A^2 - (2I_A + 1)^2}{2k_{SE}^{A-A} n_A}$, $R_{SE}^{BB} = \left(\frac{g\mu_B B}{q(0)_B \hbar} \right)^2 \frac{q(0)_B^2 - (2I_B + 1)^2}{2k_{SE}^{B-B} n_B}$, $R_{SE}^{BA} = \left(\frac{g\mu_B B}{q(0)_A \hbar} \right)^2 \frac{q(0)_A^2 - (2I_A + 1)^2}{2k_{SE}^{B-A} n_A}$, $R_{SE}^{AB} = \left(\frac{g\mu_B B}{q(0)_B \hbar} \right)^2 \frac{q(0)_B^2 - (2I_B + 1)^2}{2k_{SE}^{A-B} n_B}$, where B is the external magnetic field, $q(0)$ is the low polarization limit of the slowing-down factor, I is nuclear spin of the alkali-metal atoms. We consider the optical pumping rate of pump beam of alkali-metal atoms(³⁹K and ¹³³Cs) R_A and the pumping rate of atom B R_B , which are only related with their parameters. Buffer gas is ⁴He, quench gas is N₂, then we acquire the fundamental sensitivity of the hybrid optical pumping SERF atomic magnetometer due to the shot-noise of a probe laser as following

$$\delta B = \frac{\sqrt{\Gamma_A + \Gamma_B + R_{wall}^A + R_{wall}^B + R_A + R_B + R_{SE}^{AA} + R_{SE}^{AB} + R_{SE}^{BA} + R_{SE}^{BB}}}{\gamma_e \sqrt{n_B V t}}. \quad (8)$$

If we consider the influence of the light shift noise^{5,39} B_{LS} , photon shot noise⁸ B_{psn} , spin-projection noise⁵ B_{spn} , magnetic field noise^{40,41} B_{mag} , technology noise B_{tech} and other noise B_{other} on the SERF atomic magnetometer. Using the method of superposition of power spectral density, we can obtain the sensitivity of the hybrid optical pumping SERF atomic magnetometer as following

$$Sen = \sqrt{(\delta B)^2 + B_{LS}^2 + B_{psn}^2 + B_{spn}^2 + B_{mag}^2 + B_{tech}^2 + B_{other}^2}. \quad (9)$$

If the noises above are optimized by technology means, the sensitivity of the hybrid optical pumping SERF atomic magnetometer is approaching to the ultimate sensitivity.

We take one of the cell effective radius a , n_{He}, n_{N2} , t , cell temperature T , optical pumping rate of pump beam (R_A^K and R_A^{Cs}), external magnetic field and measurement volume V by Eq. (8) as a variable (other parameters are invariable) to obtain the results that the fundamental sensitivity of the hybrid optical pumping SERF magnetometer based ^{39}K - ^{85}Rb - ^{4}He and ^{133}Cs - ^{85}Rb - ^{4}He vary with the variable, where $n_{He} = 10^{19}\text{cm}^{-3}$, $n_{N2} = 2 \times 10^{17}\text{cm}^{-3}$, $T = 457.5\text{K}$, $R_A^K = R_A^{Cs} = 200000\text{s}^{-1}$, $a = 1\text{cm}$, $V = 1\text{cm}^3$, $t = 400\text{s}$, $B = 10^{-15}\text{T}$. Because n_K , n_{Rb} and n_{Cs} vary with T , the relationship between the fundamental sensitivity of ^{39}K (^{133}Cs)- ^{85}Rb - ^{4}He magnetometers and the number density of alkali-metal atoms (n_K , n_{Rb} or n_{Cs}) is nonlinear. At the same T , n_K , n_{Rb} and n_{Cs} are different, the fundamental sensitivity is also different. We will study the gas cell by the characteristics and properties of the microcavities⁴²⁻⁴⁴.

Figure 3 demonstrates that R_{wall} decreases rapidly when the number density of buffer gas

increases in (a). R_{wall} increases slowly when the number density of quench gas increases in (b). R_{wall} decreases slowly when the number density of buffer gas increases in (c) and R_{wall} increases when the cell temperature increases in (d). R_{wall} decreases rapidly when the cell effective radius increases in (e). The R_{wall} of ^{39}K - ^{85}Rb - ^4He magnetometer is the smallest between ^{39}K - ^{85}Rb - ^4He and ^{133}Cs - ^{85}Rb - ^4He magnetometers.

Figures 4-5 show the fundamental sensitivity of ^{85}Rb atom of ^{39}K (^{133}Cs)- ^{85}Rb - ^4He magnetometers as a function of ^{39}K , ^{133}Cs , ^{85}Rb , ^4He and N_2 number density, R_A^K and R_A^{Cs} , external magnetic field, cell temperature and measurement time, cell effective radius, measurement volume, includes the effects of spin exchange due to ^{39}K - ^{39}K , ^{39}K - ^{85}Rb , ^{85}Rb - ^{85}Rb , ^{133}Cs - ^{85}Rb , ^{133}Cs - ^{133}Cs and spin relaxation due to ^{39}K - ^{39}K , ^{39}K - ^{85}Rb , ^{85}Rb - ^{85}Rb , ^{133}Cs - ^{85}Rb , ^{133}Cs - ^{133}Cs , ^{39}K - ^4He , ^{85}Rb - ^4He , ^{133}Cs - ^4He collisions, ^{39}K - N_2 , ^{85}Rb - N_2 , ^{133}Cs - N_2 destructions.

Fig. 4(a) represents that the fundamental sensitivity of ^{39}K - ^{85}Rb - ^4He magnetometer (black line in squares) increases with the increasing number density of ^4He when ^4He number density is smaller than a critical value at about $4.915 \times 10^{19} \text{ cm}^{-3}$ and decreases when ^4He number density is higher than the value. The fundamental sensitivity of ^{133}Cs - ^{85}Rb - ^4He magnetometer (red line in dots) increases with the increasing number density of ^4He when ^4He number density is smaller than a critical value at about $3.13 \times 10^{19} \text{ cm}^{-3}$ and decreases when ^4He number density is higher than the value. For this phenomenon, we think that more alkali-metal atoms diffuse to the cell wall and less spin exchange collisions between alkali-metal atoms A and B when the number density of ^4He is smaller than the value and decrease. Less alkali-metal atoms diffuse to the cell wall

and more spin exchange collisions between alkali-metal atoms and buffer gas so that there are less spin exchange collisions in alkali-metal atoms when the number density of ${}^4\text{He}$ is bigger than the value and increase. Therefore, if we take the critical value as ${}^4\text{He}$ number density, spin exchange collisions in alkali-metal atoms are the most, we can obtain the highest fundamental sensitivity of the magnetometer.

Fig. 4(b) shows that the fundamental sensitivity of ${}^{39}\text{K} ({}^{133}\text{Cs})$ - ${}^{85}\text{Rb}$ - ${}^4\text{He}$ magnetometers almost do not vary with the increasing N_2 number density when N_2 number density is smaller than a critical value 10^{19} cm^{-3} and decrease when N_2 number density are bigger than the value respectively. The fundamental sensitivity of ${}^{39}\text{K} ({}^{133}\text{Cs})$ - ${}^{85}\text{Rb}$ - ${}^4\text{He}$ magnetometers decrease with the increasing optical pumping rate of pump beam respectively in (c). The fundamental sensitivity of ${}^{39}\text{K} ({}^{133}\text{Cs})$ - ${}^{85}\text{Rb}$ - ${}^4\text{He}$ magnetometers(black line in squares and red line in dots) increase with the increasing measurement time. The fundamental sensitivity of ${}^{133}\text{Cs}$ - ${}^{85}\text{Rb}$ - ${}^4\text{He}$ magnetometer (red line in dots) are lower than the one of ${}^{39}\text{K}$ - ${}^{85}\text{Rb}$ - ${}^4\text{He}$ magnetometer (black line in squares) in (d).

Fig. 5 describes that when the external magnetic field is smaller than 10^{-7} T , the fundamental sensitivity of ${}^{39}\text{K} ({}^{133}\text{Cs})$ - ${}^{85}\text{Rb}$ - ${}^4\text{He}$ magnetometers almost do not vary with the increasing external magnetic field respectively in (a). The fundamental sensitivity of ${}^{39}\text{K} ({}^{133}\text{Cs})$ - ${}^{85}\text{Rb}$ - ${}^4\text{He}$ magnetometers increase with the increasing cell temperature respectively and there are more spin exchange collisions in alkali-metal atoms in (b). The fundamental sensitivity of ${}^{39}\text{K} ({}^{133}\text{Cs})$ - ${}^{85}\text{Rb}$ - ${}^4\text{He}$ magnetometers increase slowly with the increasing cell effective radius respectively in (c).

The fundamental sensitivity of ^{39}K (^{133}Cs)- ^{85}Rb - ^4He magnetometers with $a = 5\text{cm}$ increase with increasing measurement volume respectively in (d). The fundamental sensitivity of ^{133}Cs - ^{85}Rb - ^4He magnetometer is lower than the one of ^{39}K - ^{85}Rb - ^4He magnetometer in (a)-(d).

As a result, the polarization of ^{85}Rb atom of the hybrid optical pumping SERF magnetometer based on ^{133}Cs - ^{85}Rb - ^4He is bigger than the one based on ^{39}K - ^{85}Rb - ^4He by Fig. 2. However, the fundamental sensitivity of ^{39}K - ^{85}Rb - ^4He magnetometer is higher than the one of ^{133}Cs - ^{85}Rb - ^4He magnetometer by figures 4-5. For another buffer gas ^{21}Ne , a large ^{85}Rb magnetization field due to spin interaction between ^{85}Rb atom and ^{21}Ne atoms causes a large spin exchange relaxation rate of ^{85}Rb atom⁴⁵ and ^{85}Rb atom can make ^{21}Ne atoms hyperpolarized, which will affect the magnetic field measurement, it is a better choice to take ^4He as the buffer gas of the SERF magnetometer to measure the magnetic field and take ^{21}Ne as the buffer gas of the SERF magnetometer to measure inertia. The fundamental sensitivity of the magnetometers based on ^{133}Cs - ^{85}Rb - ^4He is lower than the one based on ^{39}K - ^{85}Rb - ^4He .

When $n_{He} = 10^{19}\text{cm}^{-3}$, $n_{N2} = 2 \times 10^{17}\text{cm}^{-3}$, $T = 457.5\text{K}$, $R_A^K = R_A^{Cs} = 200000\text{s}^{-1}$, $a = 1\text{cm}$, $V = 1\text{cm}^3$, $B = 10^{-15}\text{T}$, $t = 400\text{s}$, the polarization of ^{85}Rb atom of the magnetometer is uniform, we obtain a fundamental sensitivity of $26.303aT/\text{Hz}^{1/2}$ with ^{39}K - ^{85}Rb - ^4He magnetometer with ^{85}Rb polarization is 0.0121 and a fundamental sensitivity of $30.309aT/\text{Hz}^{1/2}$ with ^{133}Cs - ^{85}Rb - ^4He magnetometer with ^{85}Rb polarization is 0.0435. Optimizing above parameters, we obtain a fundamental sensitivity of $1.8449 \times 10^{-2}aT/\text{Hz}^{1/2}$ with ^{39}K - ^{85}Rb - ^4He with the polarization of ^{85}Rb atom is 1.3961×10^{-5} and a fundamental sensitivity of $4.3187 \times 10^{-2}aT/\text{Hz}^{1/2}$

with ^{133}Cs - ^{85}Rb - ^4He with the polarization of ^{85}Rb atom is 5.0431×10^{-5} with $n_{He} = 10^{19} \text{ cm}^{-3}$, $n_{N_2} = 2 \times 10^{15} \text{ cm}^{-3}$, $T = 457.5 \text{ K}$, $R_A^K = R_A^{Cs} = 200 \text{ s}^{-1}$, $a = 10 \text{ cm}$, $B = 10^{-15} \text{ T}$, $V = 1000 \text{ cm}^3$, $t = 4000 \text{ s}$, with higher fundamental sensitivity possible at bigger measurement volume, lower buffer gas and quench gas number density, smaller optical pumping rate, higher temperature and longer measurement time.

Discussion

In conclusion, we find that ^{85}Rb polarization increases with the increasing optical pumping rate. The polarization of ^{85}Rb atom of ^{133}Cs - ^{85}Rb - ^4He magnetometer is bigger than the one of ^{39}K - ^{85}Rb - ^4He magnetometer. The polarization of ^{85}Rb atom of ^{39}K (^{133}Cs)- ^{85}Rb - ^4He magnetometers almost do not vary when the number density of ^4He and N_2 increase and the number density of buffer gas and quench gas are smaller than some critical values and decrease rapidly when the number density of buffer gas and quench gas are bigger than the values respectively. The fundamental sensitivity increases with the increasing number density of buffer gas when the number density of buffer gas is smaller than a critical value and decreases when the number density of buffer gas is bigger than the value. The fundamental sensitivity increases with the increasing cell effective radius, measurement volume, cell temperature and measurement time respectively. The fundamental sensitivity of the magnetometers decrease with increasing R_A^K and R_A^{Cs} . At the same cell temperature, the polarization of ^{85}Rb atom of ^{133}Cs - ^{85}Rb - ^4He magnetometer is bigger than the one of ^{39}K - ^{85}Rb - ^4He magnetometer and the magnetometers fundamental sensitivity of ^{133}Cs - ^{85}Rb - ^4He magnetometer is lower than the one of ^{39}K - ^{85}Rb - ^4He magnetometer.

To obtain a higher fundamental sensitivity of the hybrid optical pumping SERF magnetometer between ^{39}K - ^{85}Rb - ^4He and ^{133}Cs - ^{85}Rb - ^4He magnetometers, it is better to choose ^{39}K - ^{85}Rb - ^4He magnetometer, with ^4He as the buffer gas and take the critical value of ^4He number density, increase the cell effective radius, measurement volume, cell temperature, measurement time, then reduce the external magnetic field, the number density of the quench gas N_2 , the optical pumping rate of pump beam based on actual demand. We estimate the fundamental sensitivity limit of the hybrid optical pumping SERF magnetometer due to the shot-noise of a probe laser superior to $1.8449 \times 10^{-2} aT/\text{Hz}^{1/2}$, which is higher than the shot-noise-limited sensitivity of $1aT/\text{Hz}^{1/2}$ of K SERF atomic magnetometer. We could choose suitable conditions on the basis of the experiment requirements to gain a higher sensitivity of the SERF atomic magnetometer, keep the costs down and carry forward the miniaturization and practical application of the hybrid optical pumping SERF atomic magnetometers.

1. Johnson, C. N., Schwindt, P. D. D. & Weisend, M. Multi-sensor magnetoencephalography with atomic magnetometers. *Phys. Med. Biol.* **58**, 6065-6077 (2013).
2. Sander, T. H., Preusser, J., Mhaskar, R., Kitching, J., Trahms, L. & Knappe, S. Magnetoencephalography with a chip-scale atomic magnetometer. *Biomed. Opt. Express* **3**, 981-990 (2012).
3. Wyllie, R., Kauer, M., Smetana, G. S., Wakai, R. T. & Walker, T. G. Magnetocardiography with a modular spin-exchange relaxation free atomic magnetometer array. *Phys. Med. Biol.* **57**, 2619-2632 (2012).
4. Brown, J. M., Smullin, S. J., Kornack, T. W. & Romalis, M. V. New Limit on Lorentz- and CPT-Violating Neutron Spin Interactions. *Phys. Rev. Lett.* **105**, 151604 (2010).
5. Seltzer, S. J. Developments in Alkali-Metal Atomic Magnetometry. *Princeton University* (2008).
6. Kornack, T. W. A Test of CPT and Lorentz Symmetry Using a K-³He Co-magnetometer. *Princeton University* (2005).
7. Fang, J. C., Qin, J., Wan, S. A., Chen, Y. & Li, R. J. Atomic spin gyroscope based on ¹²⁹Xe-Cs comagnetometer. *Chin. Sci. Bull.* **58**, 1512-1515 (2013).
8. Ledbetter, M. P., Savukov, I. M., Acosta, V. M., Budker, D. & Romalis, M. V. Spin-exchange-relaxation-free magnetometry with Cs vapor. *Phys. Rev. A* **77**, 033408 (2008).

9. Nelson, I. A. Physics of Practical Spin-Exchange Optical Pumping. *University of Wisconsin - Madison* (2001).
10. Kominis, I. K., Kornack, T. W., Allred, J. C. & Romalis, M. V. A subfemtotesla multichannel atomic magnetometer. *Nature* **422**, 596-599 (2003).
11. Happer, W. & Tang, H. Spin-exchange shift and narrowing of magnetic resonance lines in optically pumped alkali vapors. *Phys. Rev. Lett.* **31**, 273-276 (1973).
12. Happer, W. & Tam, A. C. Effect of rapid spin exchange on the magnetic-resonance spectrum of alkali vapors. *Phys. Rev. A* **16**, 1877-1891 (1977).
13. Dong, H. F., Xuan, L. F., Zhuo, C. & Lin, H. B. Two Unshielded SERF Magnetometer Schemes and Their Comparison. *J. Test Meas. Techol.* **26**, 468 (2012).
14. Ito, Y., Ohnishi, H., Kamada, K. & Kobayashi, T. Effect of spatial homogeneity of spin polarization on magnetic field response of an optically pumped atomic magnetometer using a hybrid cell of K and Rb atoms. *IEEE T. Magn.* **48**, 3715-3718 (2012).
15. Romalis, M. V. Hybrid optical pumping of optically dense alkali-metal vapor without quenching gas. *Phys. Rev. Lett.* **105**, 243001 (2010).
16. Ito, Y., Ohnishi, H., Kamada, K. & Kobayashi, T. Sensitivity Improvement of Spin-Exchange Relaxation Free Atomic Magnetometers by Hybrid Optical Pumping of Potassium and Rubidium. *IEEE T. Magn.* **47**, 3550-3553 (2011).

17. Ito, Y., Ohnishi, H., Kamada, K. & Kobayashi, T. Rate-equation Approach to Optimal Density Ratio of K-Rb Hybrid Cell for Optically Pumped Atomic Magnetometers. *35th Annual International Conference of the IEEE EMBS* **6**, 3254-3257 (2013).

18. Fang, J. C., Wang, T., Zhang, H., Li, Y. & Zou, S. Optimizations of spin-exchange relaxation-free magnetometer based on potassium and rubidium hybrid optical pumping. *Rev. Sci. Instrum.* **85**, 123104 (2014).

19. Li, Y., Cai, H. W., Ding, M., Quan, W. & Fang, J. C. A Subfemtotesla Atomic Magnetometer Based on Hybrid Optical Pumping of Potassium and Rubidium. *47th Ann. Meet. APS DAMOP*. **61**, 8 (2016).

20. Alcock, C. B., Itkin, V. P. & Horrigan, M. K. Vapour Pressure Equations for the Metallic Elements: 298-2500 K. *Can. Metall. Quart.* **23**, 309-313 (1984).

21. Jau, Y. Y., Miron, E., Post, A. B., Kuzma, N. N. & Happer, W. Push-pull optical pumping of pure superposition states. *Phys. Rev. Lett.* **93**, 160802 (2004).

22. Shang, H. N., Quan, W., Chen, Y., Li, Y. & Li, H. The Measuring Method of Atomic Polarization of Alkali Metal Vapor Based on Optical Rotation and the Analysis of the Influence Factors. *Spectrosc. Spect. Anal.* **36**, 305-309 (2016).

23. Wu, Z., Kitano, M., Happer, W., Hou, M. & Daniels, J. M. Optical determination of alkali metal vapor number density using Faraday rotation. *Appl. Optics* **25**, 4483-4492 (1986).

24. Gibbs, H. M. & Hull, R. J. Spin-Exchange Cross Sections for Rb^{87} - Rb^{87} and Rb^{87} - Cs^{133} Collisions. *Phys. Rev.* **153**, 132-151 (1967).

25. Ressler, N. W., Sands, R. H. & Stark, T. E. Measurement of Spin-Exchange Cross Sections for Cs¹³³, Rb⁸⁷, Rb⁸⁵, K³⁹, and Na²³. *Phys. Rev.* **184**, 102-118 (1969).

26. Shao, W. J., Wang, G. D. & Hughes, E. W. Measurement of spin-exchange rate constants between ¹²⁹Xe and alkali metals. *Phys. Rev. A* **72**, 022713 (2005).

27. Ghosh, R. K. & Romalis, M. V. Measurement of spin-exchange and relaxation parameters for polarizing ²¹Ne with K and Rb. *Phys. Rev. A* **81**, 043415 (2010).

28. Quan, W., Li, Y. & Liu, B. Simultaneous measurement of magnetic field and inertia based on hybrid optical pumping. *Europhys. Lett.* **110**, 60002 (2015).

29. Kadlecak, S., Anderson, L. W. & Walker, T. Measurement of potassium-potassium spin relaxation cross sections. *Nucl. Instr. Meth. Phys. Res.* **402**, 208-211 (1998).

30. Aleksandrov, E. B., Balabas, M. V., Vershovskii, A. K., Okunovich, A. I. & Yakobson, N. N. Spin-exchange broadening of magnetic-resonance line of potassium atoms. *Opt. Spectrosc.* **87**, 329-334 (1999).

31. Walker, T. G. & Happer, W. Spin-exchange optical pumping of noble-gas nuclei. *Rev. Mod. Phys.* **69**, 629-642 (1997).

32. Allred, J. C., Lyman, R. N., Kornack, T. W. & Romalis, M. V. High-sensitivity atomic magnetometer unaffected by spin-exchange relaxation. *Phys. Rev. A* **89**, 130801 (2002).

33. Wakai, R. T. The atomic magnetometer: A new era in biomagnetism. *AIP Conf. Proc.* **1626**, 46-54 (2014).

34. Appelt, A., Baranga, B. A., Erickson, C. J., Romalis, M. V., Young, A. R. & Happer, W. Theory of spin-exchange optical pumping of ^3He and ^{129}Xe . *Phys. Rev. A* **58**, 1412-1439 (1998).

35. Franz, F. A. & Volk, C. Electronic spin relaxation of the $4^2\text{S}_{1/2}$ state of K induced by K-He and K-Ne collisions. *Phys. Rev. A* **26**, 85-92 (1982).

36. Franz, F. A. & Volk, C. Spin relaxation of rubidium atoms in sudden and quasimolecular collisions with light-noble-gas atoms. *Phys. Rev. A* **14**, 1711-1728 (1976).

37. Franz, F. A. & Sooriamoorthi, C. E. Spin relaxation within the $6^2\text{P}_{1/2}$ and $6^2\text{S}_{1/2}$ states of cesium measured by white-light optical pumping. *Phys. Rev. A* **10**, 126-140 (1974).

38. Fang, J. C., Li, R. J., Duan, L. H., Chen, Y. & Quan, W. Study of the operation temperature in the spin-exchange relaxation free magnetometer. *Rev. Sci. Instrum.* **86**, 073116 (2015).

39. Savukov, I. M. & Romalis, M. V. Effects of spin-exchange collisions in a high-density alkali-metal vapor in low magnetic fields. *Phys. Rev. A* **71**, 023405 (2005).

40. Kornack, T. W., Smullin, S. J., Lee, S. K. & Romalis, M. V. A low-noise ferrite magnetic shield. *Appl. Phys. Lett.* **90**, 223501 (2007).

41. Kubo, R. The fluctuation-dissipation theorem. *Rep. Prog. Phys.* **29**, 255-284 (1966).

42. Qi, R., Yu, X. L., Li, Z. B. & Liu, W. M. Non-Abelian Josephson effect between two F=2 spinor Bose-Einstein condensates in double optical traps. *Phys. Rev. Lett.* **102**, 185301 (2009).

43. Ji, A. C., Sun, Q., Xie, X. C. & Liu, W. M. Josephson effect for photons in two weakly linked microcavities. *Phys. Rev. Lett.* **102**, 023602 (2009).

44. Ji, A. C., Xie, X. C. & Liu, W. M. Quantum magnetic dynamics of polarized light in arrays of microcavities. *Phys. Rev. Lett.* **99**, 183602 (2007).
45. Chen, Y., Quan, W., Zou, S., Lu, Y., Duan, L. H., Li, Y., Zhang, H., Ding, M. & Fang, J. C. Spin exchange broadening of magnetic resonance lines in a high-sensitivity rotating K-Rb-²¹Ne co-magnetometer. *Sci. Rep.* **6**, 36547 (2016).

Acknowledgement We thank Y. Chen (Beihang University), J. X. Lu (Beihang University), Y. Li (Beihang University) and B. Dong (NTSC, Chinese Academy of Sciences) for discussions and communications. This work was supported by the NKRDP under grants Nos. 2016YFA0301500, NSFC under grants Nos. 19000550147, 11434015, 61227902, 61378017, KZ201610005011, SKLQOQOD under grants No. KF201403, SPRPCAS under grants No. XDB01020300, XDB21030300.

Author Contributions J.H.L. and W.M.L. proposed the ideas. J.H.L. interpreted physics, performed the theoretical as well as the numerical calculations and wrote the main manuscript. D.Y.J., L.L.W., P.S.H., W.Q., J.C.F. and W.M.L. checked the calculations and the results. All of the authors reviewed the manuscript.

Competing Interests The authors declare that they have no competing financial interests.

Correspondence Correspondence and requests for materials should be addressed to Wu-Ming Liu (email: wliu@iphy.ac.cn).

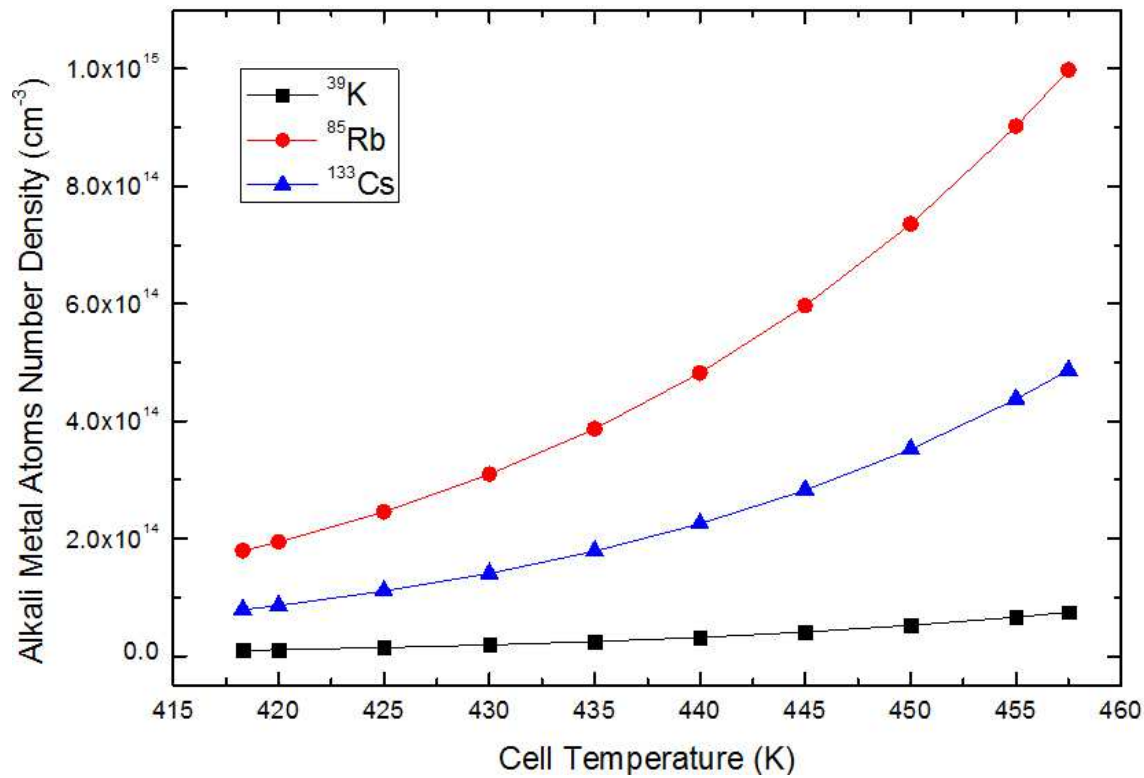


Figure 1 | The number density of ^{39}K , ^{133}Cs and ^{85}Rb vary with temperature. The effect of temperature on the number density of ^{39}K is the minimum (black line in squares), so ^{39}K is applicable to the working environment with the temperature varies drastically.

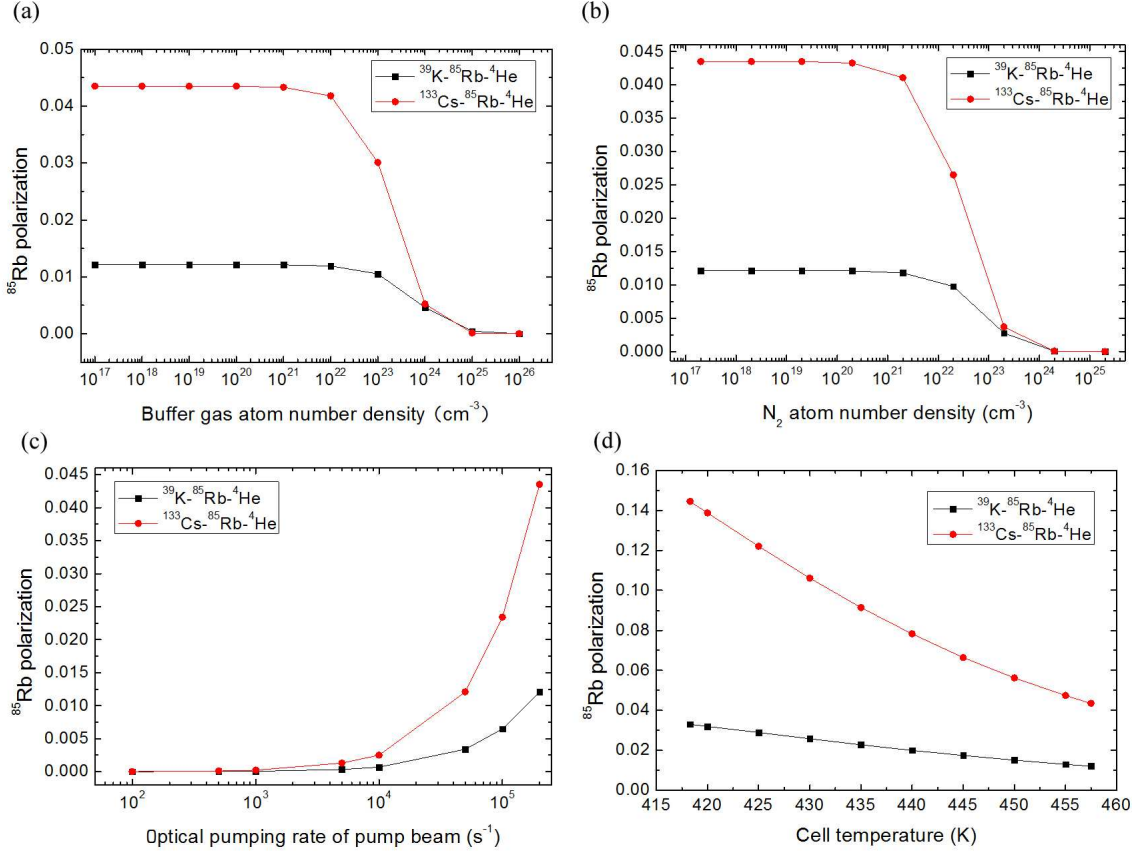


Figure 2 | The ^{85}Rb polarization of ^{39}K (^{133}Cs)- ^{85}Rb - ^4He magnetometers varies with the number density of the buffer gas (^4He), the optical pumping rate of pump beam, number density of the quench gas N_2 and the cell temperature respectively. (a) The ^{85}Rb polarization almost does not vary with the increasing number density of ^4He when the number density of ^4He is smaller than a critical value 10^{22}cm^{-3} in ^{39}K - ^{85}Rb - ^4He (black line in squares) and 10^{21}cm^{-3} in ^{133}Cs - ^{85}Rb - ^4He (red line in dots), otherwise, the polarization of ^{85}Rb atom decreases rapidly. (b) The ^{85}Rb polarization almost does not vary with the number density of N_2 when the number density of N_2 is smaller than $2 \times 10^{21}\text{cm}^{-3}$ in ^{39}K - ^{85}Rb - ^4He magnetometer and $2 \times 10^{20}\text{cm}^{-3}$ in ^{133}Cs - ^{85}Rb - ^4He magnetometer, otherwise, the ^{85}Rb polarization decreases rapidly. (c) The ^{85}Rb polarization

increases with increasing R_A^K and R_A^{Cs} respectively. (d) The ^{85}Rb polarization decreases with the increasing cell temperature. The ^{85}Rb polarization of ^{133}Cs - ^{85}Rb - ^4He magnetometer is bigger than the one of ^{39}K - ^{85}Rb - ^4He magnetometer in (c)-(d).

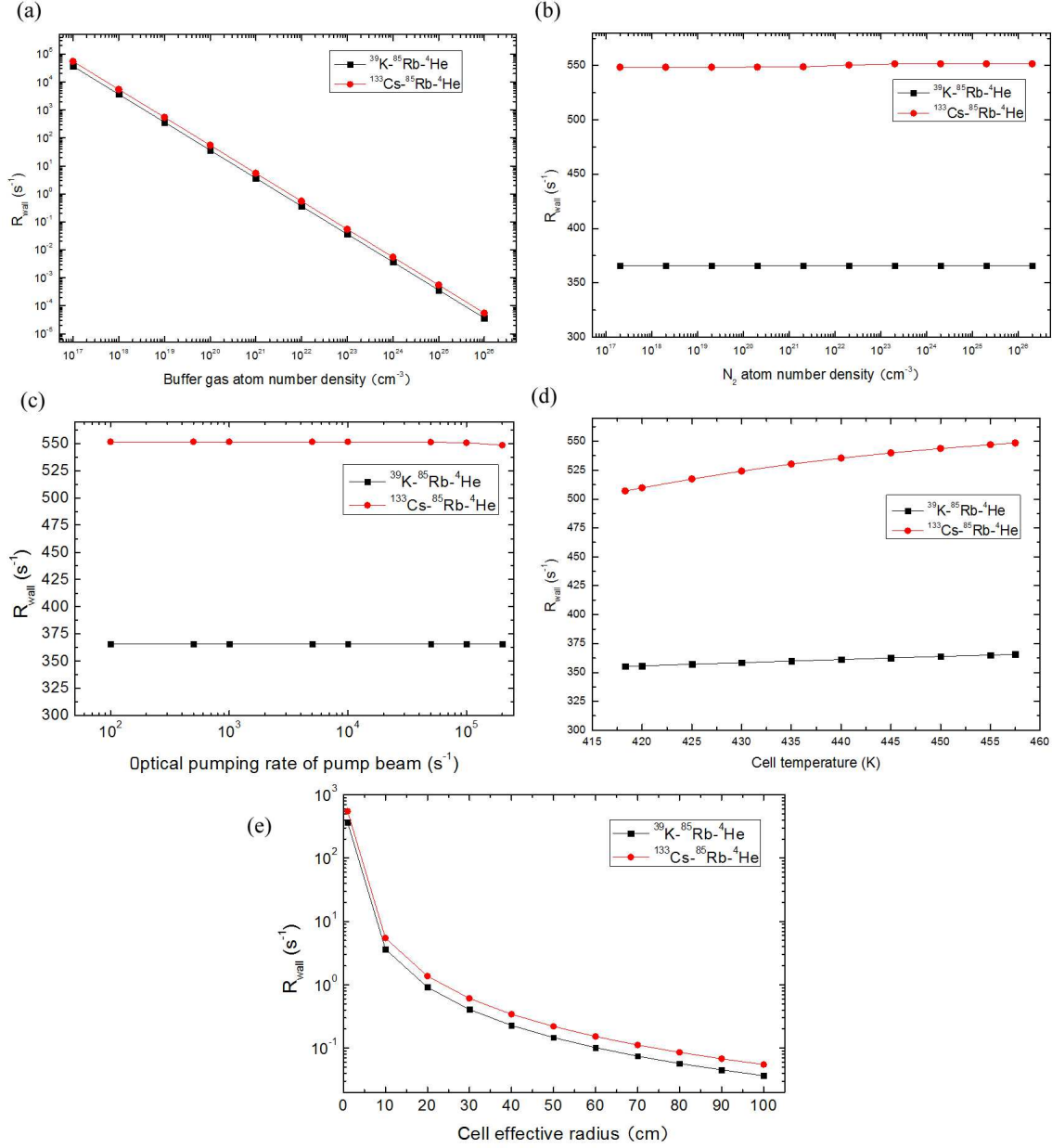


Figure 3 | The R_{wall} of ^{39}K (^{133}Cs)- ^{85}Rb - ^4He magnetometers varies with the number density of buffer gas and quench gas, optical pumping rate of pump beam, the cell temperature and cell effective radius. (a) R_{wall} decreases rapidly when the number density of buffer gas increases. (b) R_{wall} increases slowly when the number density of quench gas increases. (c) R_{wall}

decreases slowly when the number density of buffer gas increases. (d) R_{wall} increases when the cell temperature increases. (e) R_{wall} decreases rapidly when the cell effective radius increases. The R_{wall} of ^{39}K - ^{85}Rb - ^4He magnetometer is the smallest between ^{39}K - ^{85}Rb - ^4He and ^{133}Cs - ^{85}Rb - ^4He magnetometers.

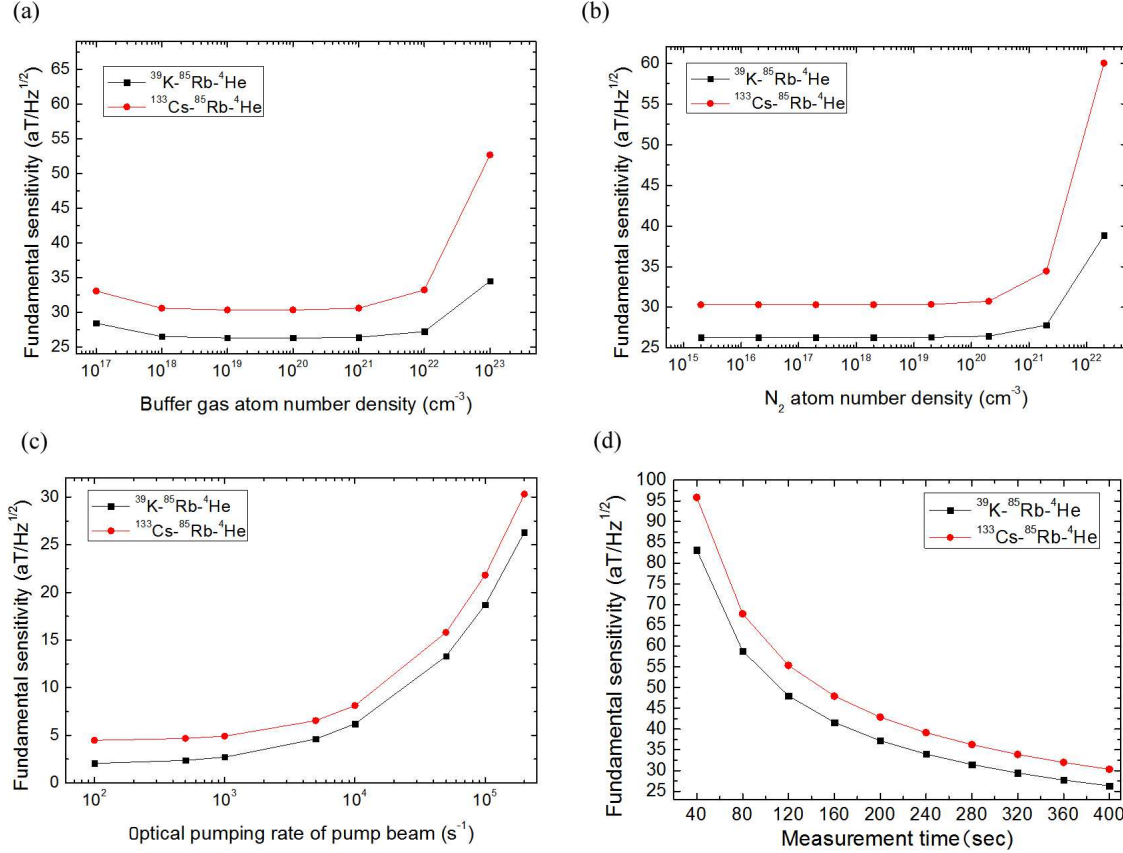


Figure 4 | The fundamental sensitivity of ^{39}K (^{133}Cs)- ^{85}Rb - ^4He magnetometers varies with the number density of buffer gas ^4He and quench gas N_2 , optical pumping rate of pump beam, measurement time. (a) The fundamental sensitivity of ^{39}K - ^{85}Rb - ^4He magnetometer (black line in squares) increases with the increasing number density of ^4He when ^4He number density is smaller than a critical value at about $4.915 \times 10^{19} \text{ cm}^{-3}$ and decreases when ^4He number density is bigger than the value. The fundamental sensitivity of ^{133}Cs - ^{85}Rb - ^4He magnetometer (red line in dots) increases with the increasing number density of ^4He when ^4He number density is smaller than a critical value at about $3.13 \times 10^{19} \text{ cm}^{-3}$ and decreases when ^4He number density is bigger than the value. (b) The fundamental sensitivity of ^{39}K (^{133}Cs)- ^{85}Rb - ^4He magnetometers almost do not

vary with increasing N_2 number density when N_2 number density is smaller than a critical value at about $10^{19} cm^{-3}$ and decrease when N_2 number density is bigger than the value respectively. The fundamental sensitivity of ^{39}K (^{133}Cs)- ^{85}Rb - 4He magnetometers decrease with the increasing optical pumping rate of pump beam in (c). The fundamental sensitivity of ^{39}K (^{133}Cs)- ^{85}Rb - 4He magnetometers increase with the increasing measurement time. The fundamental sensitivity of ^{133}Cs - ^{85}Rb - 4He magnetometer is lower than the one of ^{39}K - ^{85}Rb - 4He magnetometer in (d).

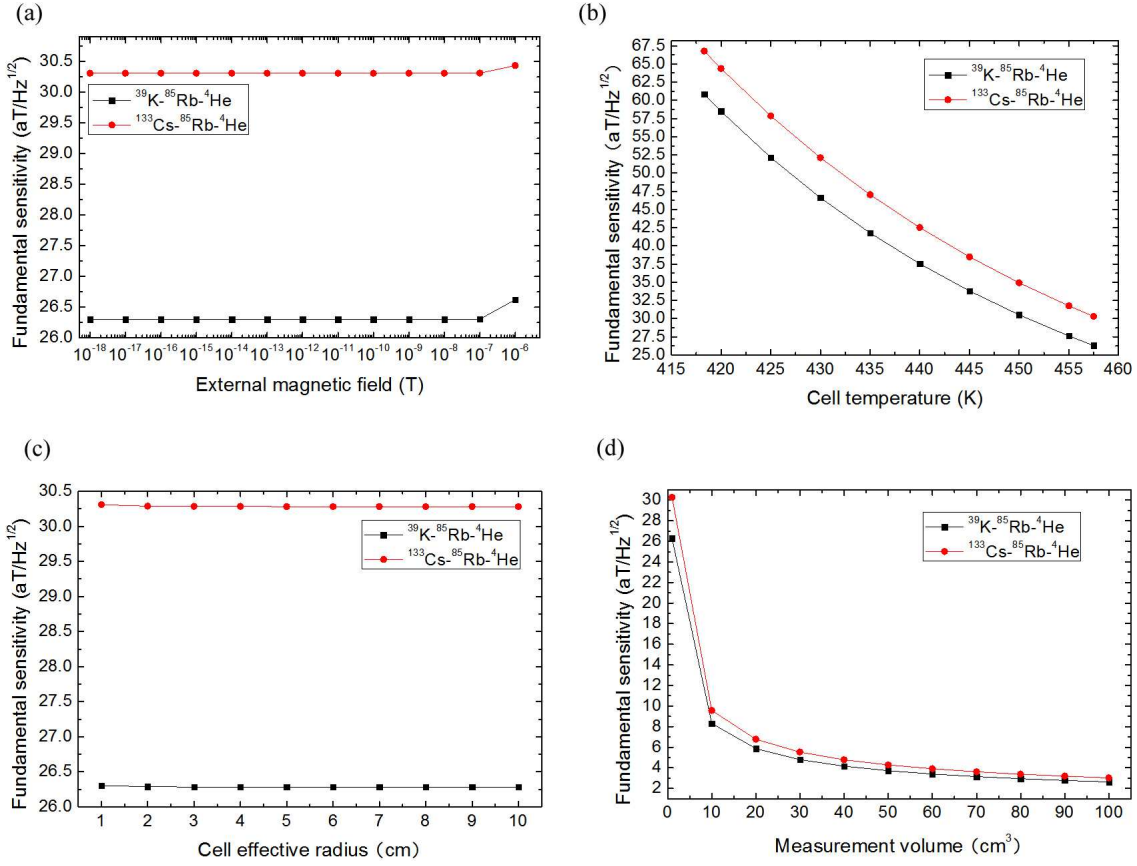


Figure 5 | The fundamental sensitivity of ^{39}K (^{133}Cs)- ^{85}Rb - ^4He magnetometers varies with the external magnetic field, cell temperature, cell effective radius and measurement volume. (a) When the external magnetic field is smaller than 10^{-7}T , the fundamental sensitivity of ^{39}K (^{133}Cs)- ^{85}Rb - ^4He magnetometers almost do not vary with the increasing external magnetic field increasing respectively. (b) The fundamental sensitivity of ^{39}K (^{133}Cs)- ^{85}Rb - ^4He magnetometers increase with the increasing cell temperature respectively. (c) The fundamental sensitivity of ^{39}K (^{133}Cs)- ^{85}Rb - ^4He magnetometers increase slowly with the increasing cell effective radius respectively. (d) The fundamental sensitivity of ^{39}K (^{133}Cs)- ^{85}Rb - ^4He magnetometers with $a = 5\text{cm}$ increase with increasing measurement volume respectively. The fundamental sensitivity of ^{133}Cs - ^{85}Rb - ^4He

magnetometer is lower than the one of ^{39}K - ^{85}Rb - ^4He magnetometer in (a)-(d).